UPPSALA
UNIVERSITET

UPTEC F 17056
Examensarbete 30 hp
November 2017

Numerical simulations of the power supply to a tidal compensation system for wave energy converters

Camilla Tumlin

UPPSALA
UNIVERSITET

Teknisk- naturvetenskaplig fakultet
UTH-enheten

Besöksadress:
Ångströmlaboratoriet
Lägerhyddsvägen 1
Hus 4, Plan 0

Postadress:
Box 536
751 21 Uppsala

Telefon:
018 – 471 30 03

Telefax:
018 – 471 30 00

Hemsida:
http://www.teknat.uu.se/student

Abstract

Numerical simulations of the power supply to a tidal compensation system for wave energy converters

Camilla Tumlin

A wave energy converter (WEC) has been developed at the Division of Electricity at Uppsala University. The Uppsala WEC is a point absorber consisting of a buoy on the surface and a linear generator situated on the sea floor. The current WEC is optimised for the wave climate at a specific location, this is however problematic in areas with large tidal variations. A compensation system adjusting the cable length according to the sea level is under development. This system is powered by rechargeable batteries which require an independent power source. One way to do this is to install a small buoy inside the main buoy which utilises the relative height between the sea level and the main buoy elevation. The small buoy can then be connected to a generator. This project concerns the design, numerical simulation and small scale experiments of a generator for this purpose. The generator function has been modelled using the finite element software and show good agreement with the experimental tests done on a simplified version. The proposed design is a linear 3-phase permanent magnet generator. Ignoring losses other than resistive losses, it converts 86% of the absorbed energy from the waves to electricity. Optimisation studies showed that the magnet and coil widths has the largest influence on the induced voltage and efficiency. There are several sources of uncertainty including other loss mechanisms, the coil inductance and the damping which depends on the exact specifications of the electrical circuit charging the batteries.

Handledare: Mohd Nasir Ayob
Ämnesgranskare: Rafael Waters
Examinator: Tomas Nyberg
ISSN: 1401-5757, UPTEC F 17056

Contents

Populärvetenskaplig sammanfattning

Utvecklandet av alternativa förnyelsebara energikällor är en nödvändighet för att ställa om vårt nuvarande fossilbaserade energisystem. En till stora delar outnyttjad resurs finns i haven där vattnets naturliga rörelser, så som vågor och strömmar, kan användas för att utvinna energi. Vid avdelningen för elektricitetslära på Uppsala Universitet har en vågenergiomvandlare utvecklats som utnyttjar havsvågors vertikal rörelser genom att låta en boj vid vattenytan driva en linjärgenerator som står på botten. Generatorn omvandlar den mekaniska rörelsen från bojen till elektrisk energi. Generatorn består av en translator med permamentmagneter som rör sig upp och ner inuti en stator med spolar. Det varierande magnetfältet från translatorns rörelse inducerar ström i dessa enligt Faradays induktionslag.

Vågenergiomvandlaren dimensioneras för ett specifikt vågklimat, detta är dock problematiskt på platser där havsnivån varierar flera meter på grund av tidvattnet. För att generatorn ska prestera optimalt behöver translatorn vara centrerad vertikalt i statorn för att absorbera all energi från vågorna. Den kabel som kopplar samman bojen och translatorn är i nuläget fix, så stora tidvattenvariationer innebär betydande förluster i form av minskad energiabsorption. Ett kompensationssystem är därför under utveckling vid avdelningen för elektricitetslära. En vinsch vevar upp eller ner en kedja och kan på så sätt justera längden på förbindelsen mellan boj och translator utefter havsnivån. För att driva vinschen används en motor och laddningsbara batterier. För att ladda batterierna behövs ett separat energiutvinningssystem. Solceller kan täcka delar av behovet, men ett komplementterande system behövs. Ett förslag är att konstruera en mindre version av ett vågkraftverk inuti vågkraftverkets huvudboj. Skillnaden mellan vattennivån och huvudbojens position i vattnet kan utnyttjas genom att ha en cylindrisk hålighet och en mindre boj på undersidan av den större bojen. Den mindre bojen rör sig därför även den upp och ner och kan på så sätt kopplas till en generator för att utvinna energi.

Detta examensarbete undersöker en möjlig konstruktion av generator givet ett visst vågklimat och begränsningar i storlek och vikt för generatorn. Projektet består i huvudsak av numeriska beräkningar för dimensioneringen av en linjär generator. Dessa har gjorts i COMSOL Multiphysics, ett simuleringsprogram baserat på finita elementmetoden. Experiment har även utförts

med en mindre, enklare version av generatorn för att delvis kunna verifiera den numeriska modellen. De experimentella testerna stämde över lag väl överens med modellen. För att få en indikation på effekten av järnet i statorn så utfördes även ett test med en smal bit järn utanpå spolen. Det hade en märkbar effekt på translatorns rörelse, vilken tenderade att då stanna av inuti spolen.

Modellen för den fullskaliga generatorn har använts för att simulera dess funktion och identifiera vilka designparametrar som påverkar mest. Den föreslagna generatorn är linjär med tre faser, bestående av en translator med permanentmagneter fastsatt på ett metallrör och en stator med sex spolar omgivna av järn. Spolarna kopplas till en elektrisk krets som likriktar strömmen och driver en last, här ett motstånd. Den föreslagna designen konverterar 86% av den inkommande energin i vågorna till elektrisk energi. Detta tar dock enbart hänsyn till kopparförluster i spolarna. Stora osäkerheter i spolarnas induktans samt andra förluster i form av friktion och virvelströmmar i järnet i statorn betyder att detta sannolikt är en övre gräns.

Ett antal olika parametrar varierades för att undersöka deras inverkan på effektiviteten. Magneternas och spolarnas bredd hade störst påverkan på den inducerade spänningen. Storlek och antal kablar som används i spolarna har också en inverkan, fler antal varv inducerar mer spänning samtidigt som det ökar resistansen och induktansen i spolarna.

Denna modell baseras på ett antal förenklade antaganden, ignorerar flera källor till förluster och har undersökt långt ifrån alla fria variabler. En betydande begränsning i modellen är att den antar att den mindre bojen kommer att röra sig på ett visst sätt (ha en fördefinierad dämpning) och sedan anpassas lasten så att det överensstämmer. Modellen kan användas som ett dimensioneringsverktyg vid sidan av konstruktionen snarare än att ge en färdig design. För den faktiska konstruktionen behöver sannolikt ytterligare ett antal restriktioner tas i beaktan.

1 Introduction

1.1 Wave power

The wave power group at the Division of Electricity at Uppsala University studies the possibilities of harnessing the energy contained in ocean waves and converting it to electrical energy. Wave energy is an active area of research and remains a largely untapped renewable energy resource. Albeit not a new concept, it has not yet seen the rapid development and deployment of some other renewable energy resources in the recent years, namely wind and solar power. The theoretical energy contained in ocean waves globally reaches the scale of PWh (10^{12} kWh) per year, but is greatly reduced when considering the technical and economical limitations [1]. The energy flux for ocean waves is predominantly given as average power per meter of wave crest. The wave resource at the coast naturally varies around the world but can reach up to 100 kW/m, while the Swedish west coast has an average energy flux of just over 5 kW/m [2].

One of the main disadvantages of wave energy is the random motion of the waves, requiring energy conversion and storage systems to smooth the power output [3]. In addition, the harsh sea environment puts high demands on the structural mechanics and materials of a wave energy converter. Thus it is also challenging to make power from ocean waves economically feasible [1]. Wave power does however have the advantage of higher energy density compared to wind due to higher density of water, the power density is 2-3 kW/m^2, which is around 5 times the energy density of wind power [4]. In addition, it has a higher utility grade (up to 90%) compared to wind and solar (20-30%) [5]. The wave power resource is also easier to predict compared to wind and has little environmental impact. Furthermore, it can be placed near demand since over a third of the world population lives within 90 km of the coast [3].

A large number of wave energy converter (WEC) prototypes have been suggested with different working principles and uses. The devices can be categorised in several different ways, for example by location such as onshore, near shore or off shore. Alternatively, by working principle such as oscillating bodies, pressure differential or overtopping devices. The most common device is the point absorber, floating devices which are small compared to

the wave length. These use the heaving or pitching motion of the waves to harness the energy. This is the type of device studied at Uppsala University (see more in the next section). Reviews of the different technologies can be found in for example Refs. [3] and [5].

Converting the energy absorbed from the waves is done by a power take-off system (PTO). There are several different ways to do this: pneumatically, hydraulically or mechanically, and in one or several conversion stages [3]. Pneumatic and hydraulic systems use a pressurised medium to convert the low frequency wave motion to high-speed motion driving a conventional rotational generator. This does however incur conversion losses and increases the complexity [6]. Mechanical PTO systems can be either direct-driven or have one or several conversion stages. A comparison of different direct-drive and linear-to-rotary PTO systems is found in Ref.[7]. In this study, modelling and lab tests showed that linear generators had highest potential in terms of energy production and cost of energy. However, material and component cost and availability are also important factors, e.g. the ability to purchase standard rotary permanent magnet generator might be more important. An alternative direct-driven energy capture system using so called dielectric elastomers is studied and tested in Ref.[8]. This systems works as a reverse "artificial muscle", where mechanical stretching of an elastomer-electrode sandwich can amplify an applied voltage (working as a capacitor with varying capacitance).

Wave energy devices exists for both electricity supply for the grid and for stand-alone applications. Small scale autonomous WECs have different requirements compared to high-power, large-scale devices. These are often studied in the context of ocean monitoring, in particular remote sensor buoys carrying various measuring equipment. These typically rely on solar panels and battery systems and/or are designed to sink when the batteries are unusable [9–11]. There are different types of autonomous WECs, for example ones converting energy using an oscillating water column (OWC) [10] or a point absorber. They can also be direct driven [12] or have a system converting linear to rotary motion [9, 11, 13].

1.2 Uppsala University WEC

The WEC developed at Uppsala University (and Seabased Industry AB) is a point absorber with a floating buoy moving with the heave of the waves. It is connected to a linear generator stationary on the sea floor, see Figure 1. A cable connects the buoy to a translator with permanent magnets on it and a voltage is induced in the windings of the stator when the buoy moves up and down. The WEC has been tested at a research site outside of Lysekil since 2004 and a large number of doctoral theses has contributed to the development, from mechanical design to grid connection [14].

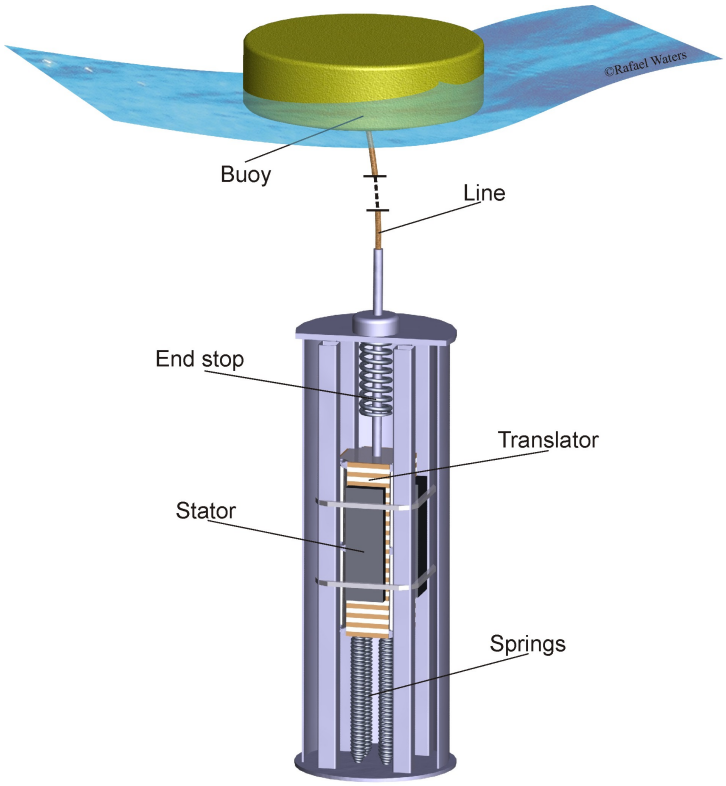

Figure 1: Sketch of the Uppsala University WEC [15].

One of the latest developments for the Uppsala WEC is studying the power absorption losses due to tidal effects, this is evaluated in Ref.[16]. The length of the cable connecting the translator to the buoy is determined by the

deployment site. However, if the site is subject to large variations in sea level due to the tide, the WEC will perform sub-optimally for large parts of the day when the cable is either slack or the buoy submerged. Areas with losses over 50% (compared to WEC without tidal compensation system) include the west coast of England and Wales, the south coast of Argentina and the north-west coast of Australia [16].

A tidal compensation system for tidal ranges up to 8 m is under development in the wave power group where a 1.5kW DC motor powers a winch used to retract or release a cable depending on the sea level [17]. The motor runs off rechargeable 12V lead acid batteries and the system requires an average of 38 W for a tidal range of 8 m. An initial study by the supervisor investigates solar panels, an oscillating water column (OWC) WEC and a small heaving point absorber WEC. This study revealed that an OWC would not be able to provide sufficient power, while the small point absorber together with solar panels could. The idea of the small point absorber WEC is that it utilises the relative difference between the wave height and the position of the main buoy, see Figure 2. The incoming wave and resulting motion of the main and small buoy is calculated numerically in MATLAB, the result can be seen Figure 3. The script was provided by the supervisor and is described in more detail in Section 2. The motion is calculated for specific wave climate and the power absorbed depends on the damping of the system. The most power absorbed by the small buoy was found to occur for a generator damping coefficient of 400 Ns/m for the most common wave, with little variation in power output above that. Figure 4 shows the average power output for different damping coefficients.

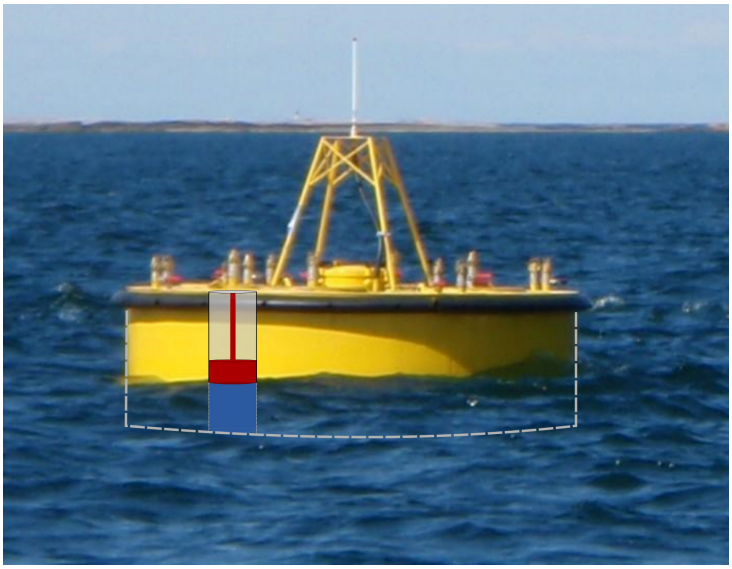

Figure 2: Illustration of a small buoy inside a larger buoy. Not to scale.

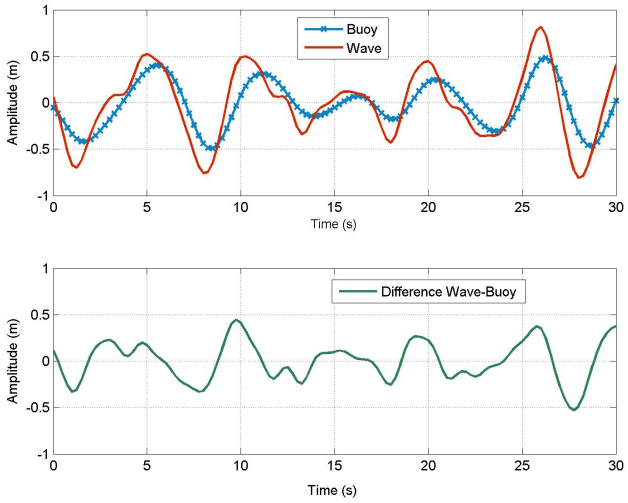

Figure 3: The incoming wave amplitude and the resulting buoy elevation on top. The difference between the two on the bottom.

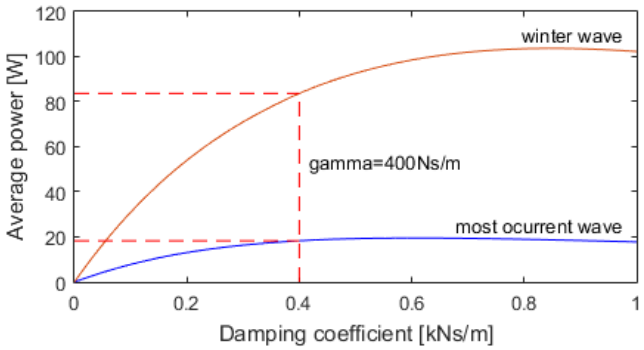

Figure 4: Power output as a function of the damping coefficient for the most common wave climate and the more energetic December wave climate. Provided by the supervisor.

1.3 Problem statement

This project concerns the energy supply for the rechareable batteries for the tidal compensation system. It focuses on designing a generator for the small buoy set-up that fits the following specifications: a maximum diameter of 35 cm, total mass of 20 kg and stroke length of 1 m. In addition, a minimum damping coefficient of 400 Ns/m is desired. In Ref.[11], a similar scale point absorber WEC in similar wave conditions was demonstrated to generate 20-50 W of power. The authors chose a rotary generator over the direct drive linear generator for efficiency reasons across different sea states. It does nevertheless show that it is feasible to obtain the desired power output using a device this size.

The design process consists of numerically simulating a linear permanent magnet generator. The numerical model is described in detail in Section 3. The simulations are done using mainly COMSOL Multiphysics, a commercial software tool used for simulating different physical problems with the finite element method. COMSOL Multiphysics enables simulation of different branches of physics within the same model, for example magnetic fields, moving or deformed geometries and structural mechanics. The electrical circuit in this project has been modelled using Simulink. Simulink is a block diagram environment integrated in MATLAB used for simulating dynamic systems.

1.3.1 Limitations

This project serves as a starting point for the design of the generator. The viability of other possible types of generators (e.g rotary) and PTO systems has not been explored. In addition, even when limiting the study to a linear permanent magnet generator the parameter space to explore is very large. Some are chosen arbitrarily and studying the effects of all of these is outside the scope of this project. A number of simplifications have naturally been made, including ignoring losses other than resistive losses in the copper windings and assuming simple air-cored coils with constant inductance. The cost and availability of components and manufacturing have not been considered in this project. The design of the support structure and buoy-generator connection has also not been included.

A major limitation in how the modelling is done is that a specific damping coefficient is assumed for the input motion of the translator. This leads to somewhat circuitous calculations. First a damping coefficient is specified which leads to a set movement of the small buoy, from this the power output and damping is calculated. The load resistance is in turn adjusted until the damping matches the specified input damping coefficient.

1.3.2 Outline of report

Following this introduction, some fundamental theory is covered in Section 2. The basic components of the numerical model is the explained in Section 3. A prototype of the generator was constructed and some experiments were performed to validate the numerical model. Section 4 describes the experiment, the adapted numerical model and the results. Following this is a more detailed description of the full-scale model for the proposed design in Section 5. Here the resulting magnetic fields, induced voltage, power output and efficiency for the model is presented. The section also includes the results from parameter variability studies. Finally, a discussion and concluding remarks are found in Section 6.

2 Theory

2.1 Water wave theory

The behaviour of ocean waves are commonly described by linear water wave theory. Conservation of mass for a fluid with density ρ and moving with velocity $\mathbf{v}$ gives the so called continuity equation:

$$\frac{\partial \rho}{\partial t} + \nabla \cdot \rho \mathbf{v} = 0. \tag{1}$$

For point absorber WECs we are interested in surface gravity waves, i.e. waves with amplitudes small compared to the depth and where gravity is the restoring force. A disturbance generating a surface deformation of a fluid in a uniform gravitational field will result in a propagating wave. The motion does not propagate far below the surface and thus one can linearize the problem assuming that the wave amplitude resulting from the displacement is small compared to the wave length [18].

Assuming ideal (ignoring viscosity) and irrotational flow of an incompressible fluid (ρ is constant), the continuity equation reduces to

$$\nabla \cdot \mathbf{v} = 0. \tag{2}$$

Defining a velocity potential $\mathbf{v} = \nabla \phi$ we can write Eq.(2) as

$$\nabla^2 \phi = 0. \tag{3}$$

The vertical displacement from a mean sea level of a small amplitude wave propagating in two dimensions can be described by the free surface $\eta(x,t)$, see Figure 5. Applying appropriate dynamic and kinematic boundary conditions on the surface and the bottom relating η and ϕ, Eq.(3) can be solved for $\eta(x,t)$. Details can be found in for example Ref.[18], the result can be written

$$\eta(x,t) = \frac{H}{2} \tan(kh) \cos(kx - \omega t). \tag{4}$$

Here H is the wave height, $h(x)$ is the depth, k the wave number and ω the angular frequency. For tidal variations one can superimpose a low frequency wave with a period matching that of the tidal cycle [1].

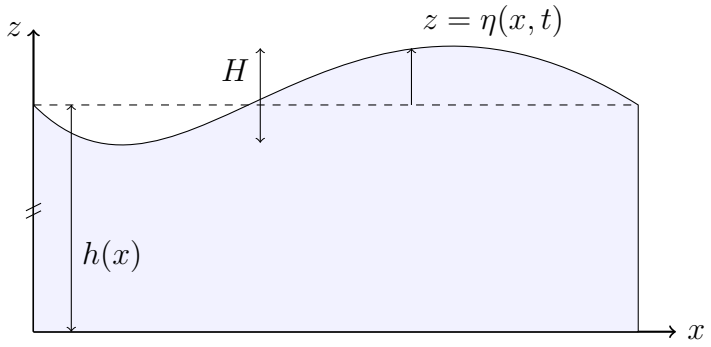

Figure 5: Surface gravity waves propagating in one dimension.

2.2 WEC model for a point absorber

A point absorber can convert energy from the wave using the heaving and pitching motion, however, a point absorber like the Uppsala WEC where the buoy is connected to a linear generator on the bottom only absorbs power through the heave motion. The power absorbed depends both on the characteristics of the point absorber and the PTO system providing the damping [6].

The vertical acceleration $\ddot{z}$ of the point absorber (buoy and translator with mass m) assuming a stiff cable connection is given by Newton's second law as:

$$m\ddot{z} = F_g + F_{gen} + F_{buoy} \tag{5}$$

where F_g is the force due to gravity, F_{gen} the damping force from the generator and F_{buoy} is the hydrodynamic force on the buoy [19]. If the generator has springs or end stops at the bottom or top, these would also be present in the above expression. The damping force is given by

$$F_{gen} = -\gamma\dot{z}, \tag{6}$$

where the damping coefficient γ is in general dependent on both the velocity and the position of the translator [20].

The hydrodynamic force on the buoy is divided into three contributions, excitation (F_e), radiation (F_r) and hydrostatic (F_h) [19]:

$$F_{buoy} = F_e + F_r + F_h. \tag{7}$$

For a cylindrical buoy with radius a we have

$$F_h = -\rho g \pi a^2 z \tag{8}$$

and the Fourier transforms of F_e and F_r as

$$\hat{F}_e(\omega) = \hat{f}_e \hat{\eta} \qquad \hat{F}_r(\omega) = -(R + i\omega m_a)\hat{\dot{z}}. \tag{9}$$

The parameters R, m_a and $\hat{f}_e$ are functions of ω and are obtained from the simulation software WAMIT. The incoming wave data is generated randomly given input location specific input parameters: the energy period T_e and the significant wave height H_s [19].

Taking the Fourier transform of Eq.(5) and substituting in the expressions for the forces we can write

$$\hat{z} = \hat{H}(\omega)\hat{\eta}(\omega) \tag{10}$$

where $\hat{H}$ is then identified as the transfer function from the amplitude of the incoming wave, the free surface $\hat{\eta}$, to the buoy elevation $\hat{z}$. In the time domain the buoy elevation $z(t)$ is then the convolution between the transfer function $H(t)$ and the incoming wave function $\eta(t)$

$$z(t) = H(t) * \eta(t). \tag{11}$$

Thus, the motion of the buoy can be determined given the incoming wave function and the transfer function which depends on the WEC specifications and the damping of the PTO system.

Having solved for the buoy elevation, the power extracted during the time from 0 to t seconds can be found using [19]

$$P(t) = \frac{1}{t}\int_0^t \gamma \dot{z}^2 dt. \tag{12}$$

2.3 Electromagnetism

The fundamental equations governing electromagnetic phenomena are Maxwell's equations. These equations reflect the fact that charge densities (ρ) and currents ($\mathbf{J}$) are the sources for the electromagnetic fields $\mathbf{E}$ and $\mathbf{B}$ [21]. In differential form they are given as follows

$$\begin{cases} \nabla \cdot \mathbf{E} = \dfrac{\rho}{\varepsilon_0} & (13) \\ \nabla \cdot \mathbf{B} = 0 & (14) \\ \nabla \times \mathbf{E} = -\dfrac{\partial \mathbf{B}}{\partial t} & (15) \\ \nabla \times \mathbf{B} = \mu_0 \mathbf{J} + \varepsilon_0 \dfrac{\partial \mathbf{E}}{\partial t} & (16) \end{cases}$$

The reciprocal relationship, i.e. the effect of the fields on a charge q moving with velocity $\mathbf{v}$ is given by the force law

$$\mathbf{F} = q\left(\mathbf{E} + \mathbf{v} \times \mathbf{B}\right). \tag{17}$$

The underlying principle behind electric machines in general, and permanent magnet generators in particular Faraday's law, Eq.(15). It states that a time-varying magnetic field (RHS of Eq.(15)) induces an electric field according (LHS of Eq.(15)). The total magnetic flux over an area $\mathcal{S}$ is

$$\Phi(t) = \int_{\mathcal{S}} \mathbf{B}(t) dA. \tag{18}$$

Using Stokes theorem to rewrite Eq.(15) and Eq.(18) we find that in a closed conductor, a change in the flux Φ of $\mathbf{B}$ through the enclosed area of the conductor induces a voltage V_{ind}:

$$V_{ind} = -\frac{d\Phi}{dt}. \tag{19}$$

The induced current in the loop will flow in the direction so as to oppose the change in the magnetic field, this is known as Lenz's law [21].

In fact, any material with free conduction electrons subject to a changing magnetic field will have currents induced within the material, so called eddy currents. These currents will as above flow so as to oppose the change and thus giving rise to an opposing force. This phenomenon is applied in for example magnetic brakes and metal detectors [22]. However, for generators this is a source of unwanted damping and power loss. The effects of eddy currents are difficult to calculate but can be reduced by for example laminating a material to reduce the available path length of the circulating currents [21], see more in the section on permanent magnets generators below.

2.3.1 Magnetic materials

A ferromagnetic material is a material that retains its magnetisation without an external magnetic field. Magnetisation of a ferromagnetic material is due to the alignment of dipoles associated with the quantum spins of unpaired electrons. In a ferromagnet these dipoles line up with their neighbours and form tiny domains where they all have the same direction. The domains are randomly distributed so that no macroscopic magnetisation occurs. However, if an external magnetic field is applied, the domains boundaries move and if the external field is strong enough the material becomes saturated, with only one domain remaining, this is a permanent magnet. It is not enough to reduce the magnetic field to zero to demagnetise the material, it requires an external magnetic field to be applied in the opposite direction [21]. This process of magnetisation and demagnetisation traces out a so called hysteresis loop, seen in Figure 6. Changing the direction of the magnetisation requires energy and a ferromagnetic material can be soft or hard depending if this process requires a small or large amount of energy respectively.

2.4 Permanent magnet generators

Permanent magnet generators can be either rotary or linear, consisting of a stator and either a rotor (rotary generators) or translator (linear generators), coil windings and an arrangement of permanent magnets. The relative motion of the permanent magnets with respect to the coils will produce a changing magnetic field, inducing a current in the coil windings according to Eq.(19).

Outside of the coils there are commonly a soft iron backing and teeth

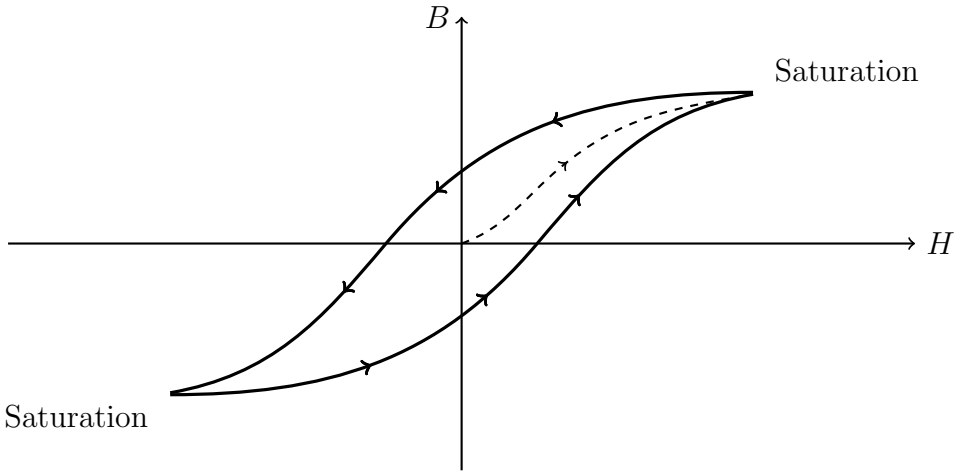

Figure 6: Hysteresis loop for a ferromagnetic material. The dashed line shows the initial magnetisation from a non-magnetised material.

in between the coils to guild the magnetic flux. However, the teeth can cause undesired attraction and cogging forces (i.e. the magnets clinging to the stator teeth), consequently putting high demands on support structures [4, 23]. Calculating the cogging force and normal force in the air gap for designing the support structure can be done analytically or using FEM, see for example Ref.[24]. For magnets with remanent flux density B_r and relative permeability μ_r the air gap flux density B_a can be calculated as

$$B_a = \frac{B_r l_{pm} \mu_r}{l_{ag} + (l_{fe} A_{ag}/\mu_{fe} A_{fe}) + (l_{pm} A_{ag}/\mu_r A_{pm})}. \tag{20}$$

Here l and A are the path length and cross sectional area of the flux through the air gap, permanent magnet and iron (subscripts ag, pm and fe respectively).

There are different types of losses present in a generator: losses from friction between the mechanical parts, copper losses in the coil windings, hysteresis losses (changing magnetisation of the materials as discussed above) and eddy current losses [20, 25]. The copper losses are dominant for low speed, low frequency applications [20]. While it is possible to reduce losses in coils by switching inactive coils off [26], it does require many power electronic components. The power loss in the coils is given by the current and

the resistance of the windings according to Ohm's law.

The hysteresis losses depend on the material, magnetic flux density and the frequency, and the per volume power loss can be estimated as [25]

$$p_{hysteresis} = k_h B_{max}^2 \omega \tag{21}$$

where k_h is a material parameter, B_{max} is the maximum magnetic flux density and ω the angular frequency. The losses from one period is given by the area of the hysteresis loop for the material as in Figure 6.

Significant losses due to eddy currents in a stator steel backing can be greatly reduced when using laminated steel [25]. The per volume eddy current losses in a laminated material with conductivity σ can be estimated using the formula [27]

$$p_{eddy} = \frac{\sigma \omega^2 d_{lam}^2 B_{max}^2}{6} \tag{22}$$

where d_{lam} is the thickness of the laminates (valid assuming the laminates are thinner than half the skin depth of the material).

2.5 Electrical damping circuits

The damping from the PTO depends on both the generator properties and load control strategy. The control can be active (using wave prediction) or passive (optimised for a given sea state) and can be done in numerous different ways. The review in Ref.[6] concluded that the optimal damping circuit will depend on the specific WEC design as well as the sea state. Experimental tests for different loading circuits has been done in Ref.[14].

A direct drive point absorber WEC can be represented by an equivalent electrical circuit model. In Figure 7 one can identify the following: Wave excitation is represented by voltage V, mass of the device represented by inductance L, mechanical damping by resistance R and if a spring is attached then the reciprocal of the spring stiffness is represented by capacitance C. The impedance Z_{PTO} represents the load from the PTO system [28].

The load resistance determines the damping from the electrical system and this needs to be tuned right: too high means less damping (thus less

power) and too low results in high dissipation in generator windings [6]. The electrical damping force F_{em} (in the opposite direction to the velocity) can be written

$$F_{em} = \frac{P_{tot}}{\dot{z}} \tag{23}$$

where P_{tot} is the total power absorbed in the generator. The equivalent circuit of a 3-phase generator and a diode bridge rectifier connected to a resistive load is shown in Figure 8. For a 3-phase circuit, the damping coefficient is found to be [29]

$$\gamma = 3\left[\frac{1}{R_g}\left(\frac{V_g}{\dot{z}}\right)^2 + \frac{1}{R_{load}}\left(\frac{V_{load}}{\dot{z}}\right)^2\right]. \tag{24}$$

However, γ is commonly assumed to be independent of $\dot{z}$ for highly resistive loads ($R_L >> R_g$) [29].

The internal resistance of the generator mainly consists of the resistivity of the conductors in the coils, thus dependent on the properties of the coil windings. The generator inductance will vary with the magnetic flux and the current in the circuit [14]. Efforts have been made to try and estimate the inductance of the coils in a linear permanent magnet generator [30] and general stacked multi-layer coils [31]. As a first order approximation, the inductance of the coils can be estimated using

$$L = \mu_0 \mu_r \frac{N_{turns}^2 A_{coil}}{l} \tag{25}$$

where N_{turns} is the number of turns, A_{coil} is the coil area and l is the length of the coil [22]. This assumes a fixed core with a material having relative permeability of μ_r inside the coil.

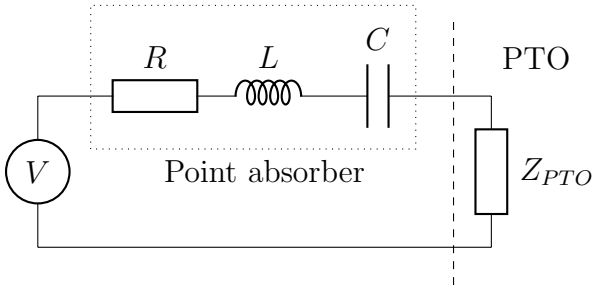

Figure 7: Equivalent circuit model for a WEC and PTO system.

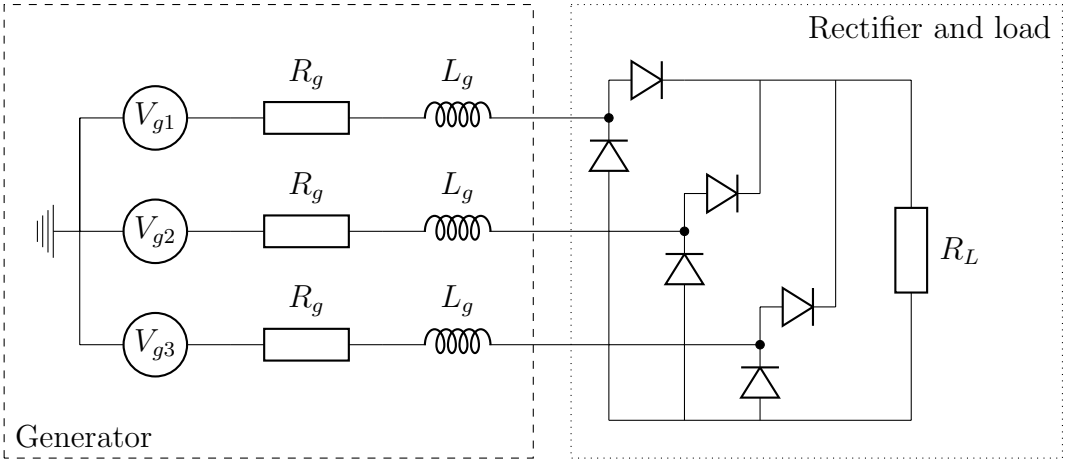

Figure 8: Equivalent circuit for a 3-phase generator connected to a full-wave diode rectifier and a single resistive load R_L. V_g is the voltage induced in the coils, R_g the resistance in the copper wires and L_g the inductance of the coils.

2.6 Finite element method

Many physics phenomena are described by partial differential equations that are often inherently difficult or impossible to solve analytically except for special cases. A well-used numerical method is the finite element method (FEM). This method was first applied to structural mechanics problems but has since been expanded to any area where solving partial differential equations is involved. FEM calculations can be very computationally expensive, especially for complex geometries, but rapidly increasing computing power becoming available in the last few decades has enabled a widespread uptake and increasing number of applications [32].

The basic idea behind finite element methods is to divide a geometry into a discrete number of subdomains (finite elements) and use numerical methods to find an approximate solution to the required equations [32]. An unknown continuous function $f(x)$ can be written as a linear combination of a set of basis functions $\{\phi\}$ and approximated by the finite sum

$$f(x) \approx f_h(x) = \sum_i c_i \phi_i \tag{26}$$

where c_i are unknown coefficients to be solved for. An example of an approximated function $f(x)$ using five elements is shown in Figure 9. Using the basis functions, a method can be formulated to obtain a system of linear equations which, with appropriate boundary conditions, can be solved numerically.

In order to ascertain that the approximate finite element solution is good enough a convergence study is required. The mesh is made successively finer until the solution is considered converged, with the requirement for convergence is dependent on the problem at hand. The element order (degree of the basis functions) can also be increased to obtain a more accurate solution.

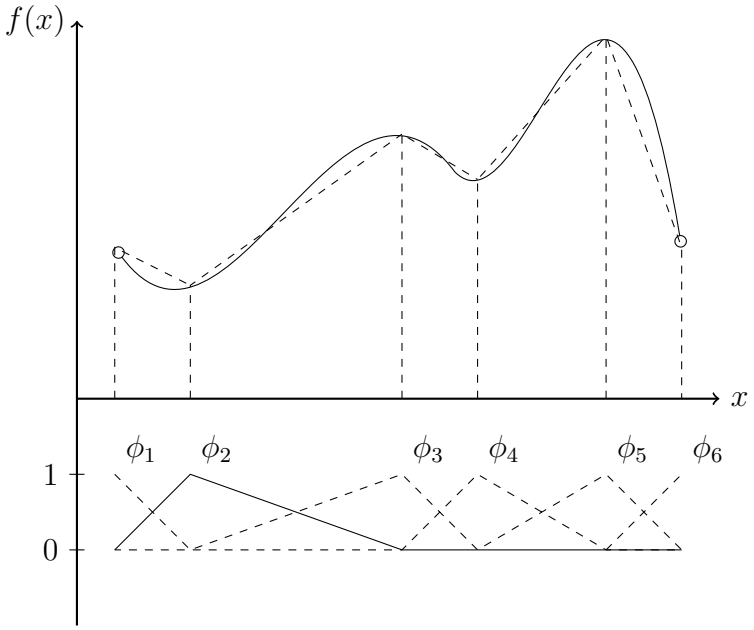

Figure 9: An arbitrary function $f(x)$ and the approximation $f_h(x)$ using linear elements. The basis functions are plotted below, with ϕ_2 drawn with a solid line for visualisation purposes.

3 Numerical modelling

The main focus of this project is the numerical modelling and will be described in general terms below. Section 4 will then describe the specific model used for the experimental prototype tests. Following that, Section 5 will discuss the simulation results for the full size generator.

The generator design is tubular so that a 2D axisymmetric (rotational symmetry) set-up can be used for the simulations. This reduces the complexity and computing time significantly compared to a full 3D geometry. The tubular design has been studied for example in Refs. [4, 23, 33, 34] and has some advantages over designs with flat sides [35], for example a better force to weight ratio [36]. However, for this project the main reason is computational considerations.

3.1 COMSOL Multiphysics

The model is built in COMSOL Multiphysics by drawing the geometry, constructing the mesh and adding physical properties on a 2D cross section in the rz-plane (the z-axis is in the axial direction of the generator). The generator consists of a core tube with magnets mounted on it, coil windings and a soft iron backing. The magnets and core tube make up the translator. The different parts of the model are shown in Figure 10.

The magnets in the model are assumed to be solid rings due to the cylindrical symmetry. However, they will in reality be individual rectangular magnets mounted on the outside of the core tube, see Figure 10. A factor R_{fac} adjusting the remanent flux density of the magnets is added to account for this difference. This factor depends on the number of magnets used, their size and the size of the inner tube, see more on this in Section 4 where the experimental test is described.

The stator consists of six coil windings, three phases connected in series. The coils are assumed to consist of insulated stranded cables with a specified diameter. The number of coil turns depends on the coil area and the cross section area of the cables. A filling factor of 0.9 is added since it is not possible to fill the entire space. Between the coils there are iron teeth and an iron backing is wrapped around the outside of the coils.

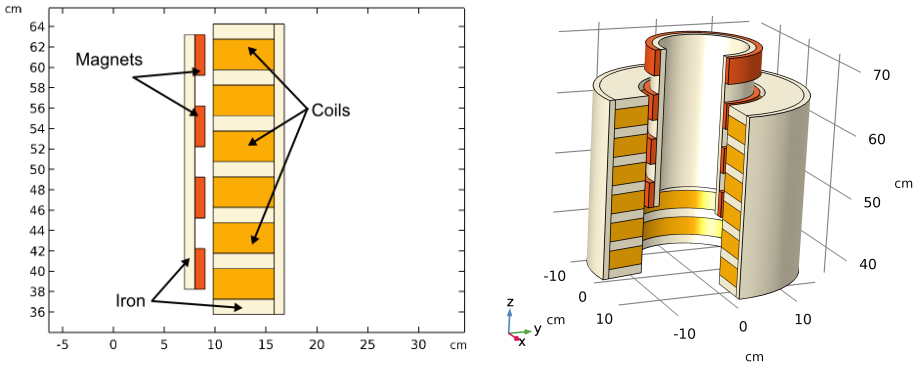

Figure 10: 2D axisymmetric and 3D view of the geometry of the generator showing the different parts

3.1.1 Materials

The properties of the magnets are given by data sheets from the supplier. The stator iron is assumed to be soft iron (to reduce hysteresis losses) using the built-in material properties COMSOL provides. The baseline simulations have been done assuming zero electrical conductivity in the soft iron.

3.1.2 Physics modelling

In COMSOL, modules are added for modelling different branches of physics. To model the magnetic fields, current densities and coils, the Magnetic Fields module is used. Here the magnetic properties of the materials are specified. The constitutive relation for the soft iron is given by the BH-curve and for the magnets by the remanent flux density. The coil properties are also defined here, for example the number of turns and the coil wire cross sectional area, as well as appropriate boundary conditions.

Since the magnets are moving, the Moving Mesh module is added where the position of the magnets are specified. The position is obtained from the provided MATLAB model, described in Section 2. The wave motion over a 10 second interval for three different damping coefficients is shown in Figure 11.

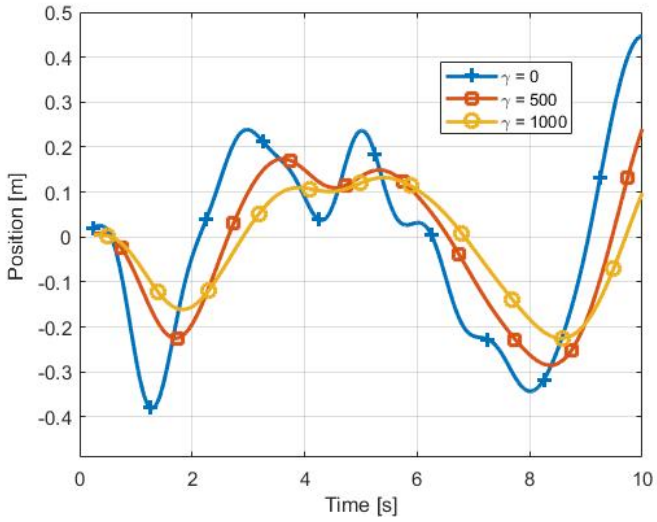

Figure 11: The vertical position of the small buoy for different damping coefficients γ (Ns/m).

3.1.3 Meshing and convergence

For this model a triangular mesh is constructed with finer mesh for the magnets, coils and iron, see Figure 12. The final size of the mesh and the order of the elements has been determined in a convergence study. A stationary solver was used to calculate the average z-component of the magnetic flux density over the coils for different sizes of the mesh. Figure 13 shows a well-converged solution for the quadratic and cubic solver using a mesh refinement factor of 2 and above. This is partly so since the geometry (in particular the air gap) necessitates a relatively fine mesh in that area for all cases. The quadratic element order with a mesh refinement factor of 2 was used for all subsequent simulations since this is considered to be converged and not too computationally time consuming.

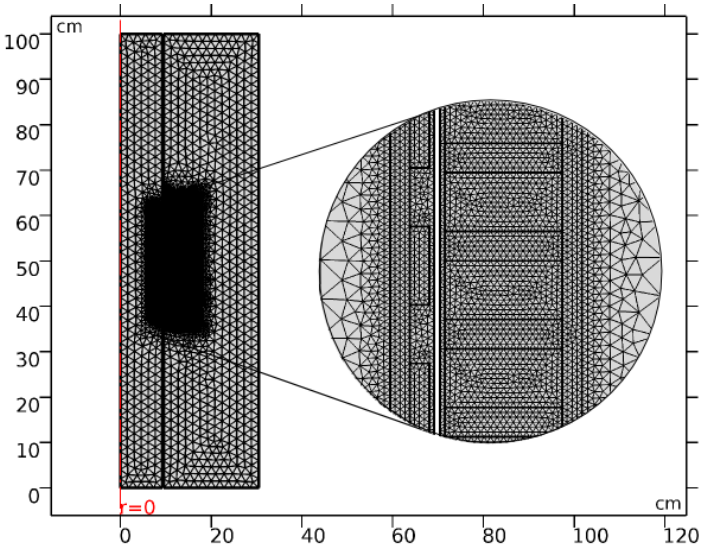

Figure 12: The mesh used for the simulations.

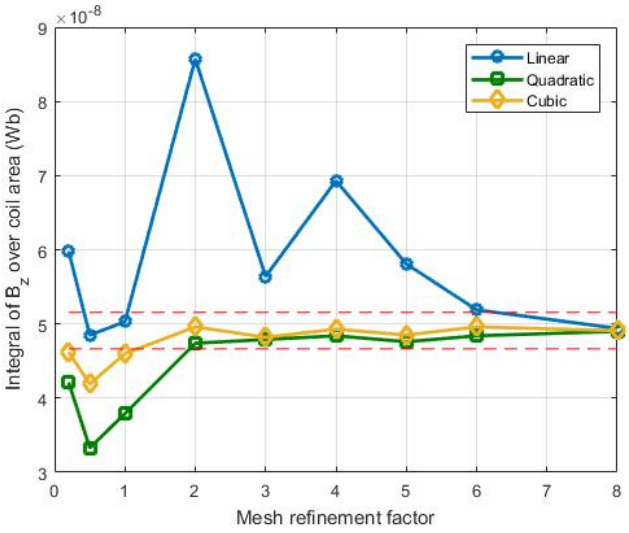

Figure 13: z-componenet of the magnetic flux density over the coils for different orders of the mesh elements and different mesh sizes. The dashed lines show $\pm 5\%$ of the final value.

3.2 Simulink: Electrical circuit model

The induced voltage from each coil group was exported from COMSOL to Simulink. The generator is modelled as a voltage source with the voltage time series from COMSOL in series with a resistor (with resistance set to the coil resistance obtained from COMSOL) and an inductor with inductance estimated from Eq.25. A full-wave rectifying circuit with a purely resistive load is connected to the generator circuit equivalent as in Figure 8. The Simulink model is shown in Figure 14. The load resistance is adjusted in an iterative process using a MATLAB script so that the damping (calculated from the power) matches the assumed input damping. The efficiency can then be calculated.

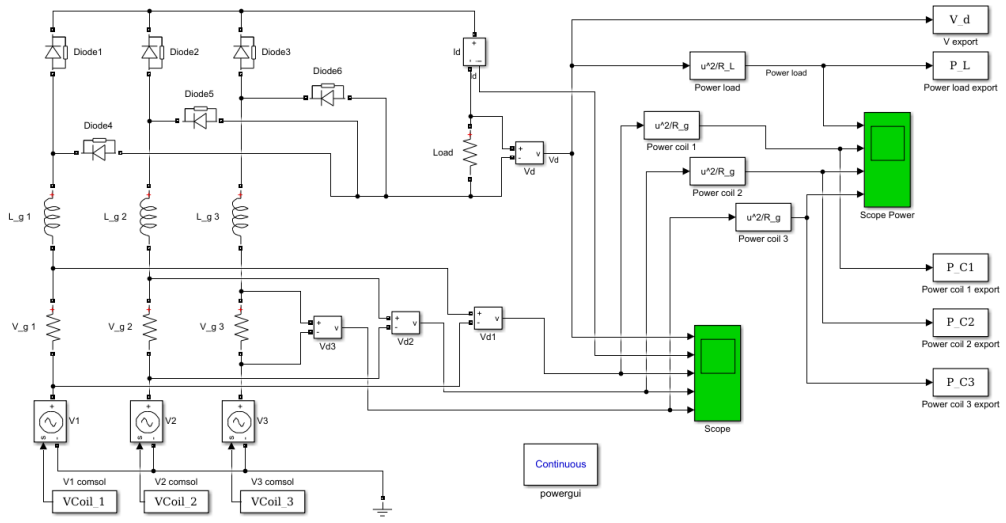

Figure 14: Simulink model of rectifying circuit for the generator

4 Prototype experiment

To ensure that the numerical model is a good representation of a real generator, a small scale and simplified version of the generator was constructed. The induced voltage was measured and compared to that predicted by a corresponding COMSOL model.

4.1 Experimental set up

The translator consists of a steel cylinder with magnets placed on the outside in two rows of 17 magnets each. A cord attached to the translator enables it to be moved vertically by hand. The stator consists of a cable wound around a plastic tube to make the coil. A cardboard tube is fitted inside the coil to be able to move the translator smoothly up and down. See pictures of the experimental set up in Figure 15.

Table 1: Parameters for the experimental set up

Magnet dimensions	15x15x8 mm
Number of magnets	34 in 2 rows
Remanent flux density	1.3 T
Core tube diameter	8.9 cm
Core tube thickness	3 mm
Air gap	5 mm
Cable diameter	1 mm copper
	2 mm incl. insulation
Coil height	6 cm
Coil width	5 mm
Coil diameter	12.3 cm
Number of turns	107

The induced no load voltage was measured with an oscilloscope. The translator was pulled upwards from the bottom position (on the floor) to the top of the tube (the translator moves from well below to well above the coil). The position of the translator was measured using a draw-wire displacement sensor. A linear fit of the position measurement was used to obtain the speed, this was then used as input in the numerical model. The motion of the small

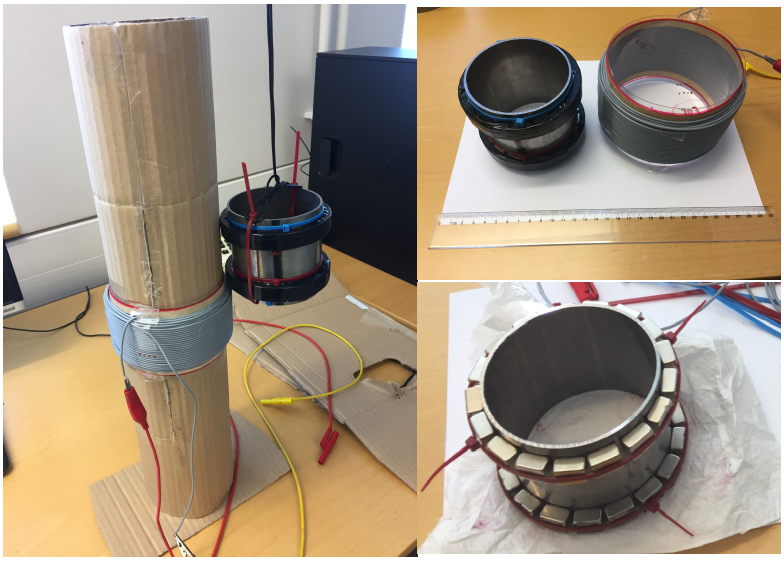

Figure 15: Experimental set up. Left: Finished prototype. Right: Top shows translator (left) and coil (right) and bottom shows the individual magnets being attached to the translator.

buoy (see Figure 11) has a maximum speed of 0.62 m/s with a mean speed of 0.16 m/s. Two different tests were conducted with different average speeds: 0.48 and 0.89 m/s.

4.2 Numerical model

The different parts of the numerical representation of the experimental set up is shown in Figure 17. The numerical model is a 2D axisymmetric model, meaning that everything is assumed to have cylindrical symmetry. This includes the magnets, which are modelled as solid rings rather than individual magnets. A separate full 3D model was made to study the differences between the two cases, considering only the steady state magnetic fields. The two different geometries can be seen in Figure 16. The 3D model was used to calculate the difference in magnet volume between the two cases. The resulting magnetic flux in an iron tube surrounding the magnets was also calculated and compared for the two cases. The resulting magnetic flux density and magnetic field lines are shown in Figure 18. We can see that the top magnets are magnetised in the negative r-direction and the bottom

magnets in the positive direction. The small magnets was found to have a volume of 0.84 times that of the solid magnets, while the ratio for the magnetic flux density wass 0.85. Adjusting the remanent flux density of the solid magnet by this factor reduces the magnetic field in the iron by the same factor. Therefore, when modelling the induced voltage, B_0 is multiplied by 0.85.

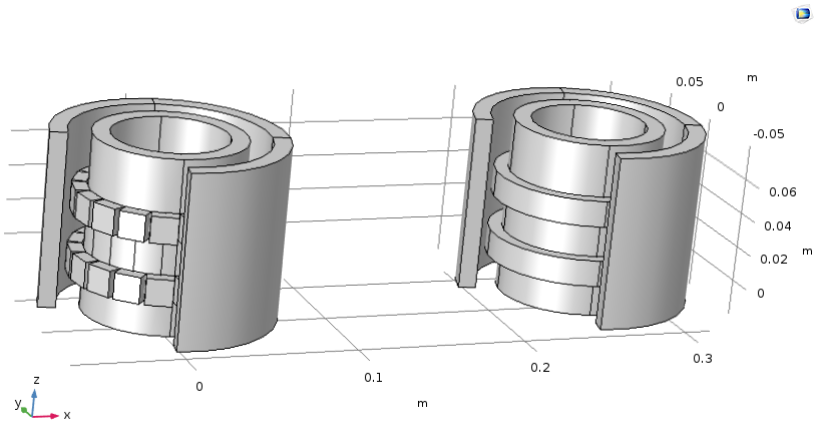

Figure 16: Drawn geometries using small magnets (left) and solid ring magnets (right).

4.3 Experimental results

The position measurement and a linear fit (using MATLAB's built in least square functionality) can be seen in Figure 19. The induced voltages obtained from the measurement and from the numerical model is shown in Figure 20. The graph of the calculated voltage has been shifted so that the zero crossing between the peaks (when the translator is exactly in the middle of the coil) occurs at the same time as the one for the measured values. The calculated voltage predicts higher initial peaks before the main peaks and the second peak is larger and somewhat skewed compared to the measured values. In general it provides a reasonably good estimate. The effect of the difference in magnet volume is not significant, but seems to be well accounted for by adding the factor R_{fac} to the remanent flux density of the magnets. Figure 21 shows the induced voltage for the case where the translator moves with speed 0.89 m/s.

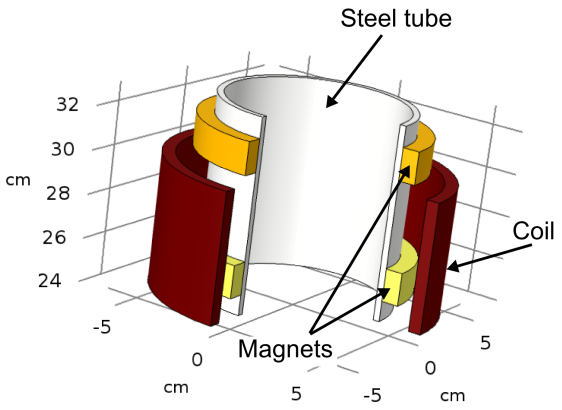

Figure 17: The different parts of the prototype model.

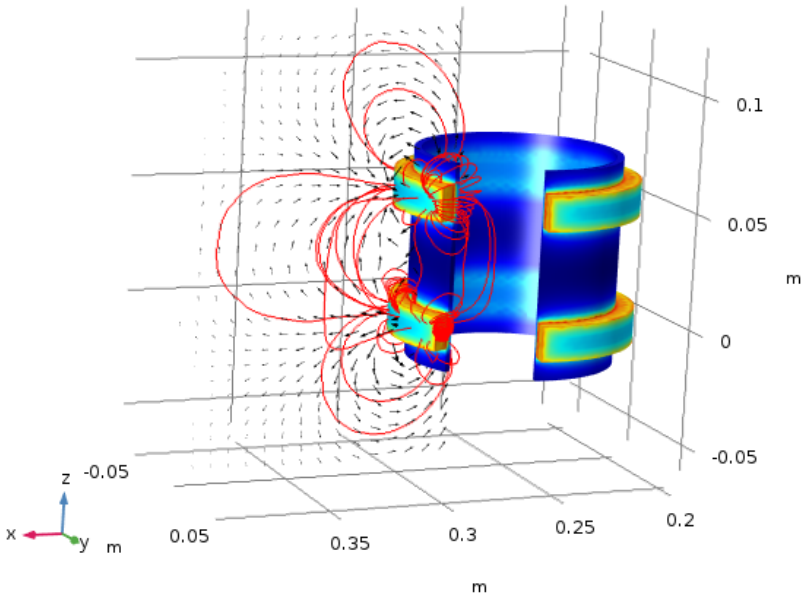

Figure 18: Magnetic flux density for the magnets. The top ring is magnetized in the negative and the bottom one in the positive radial direction.

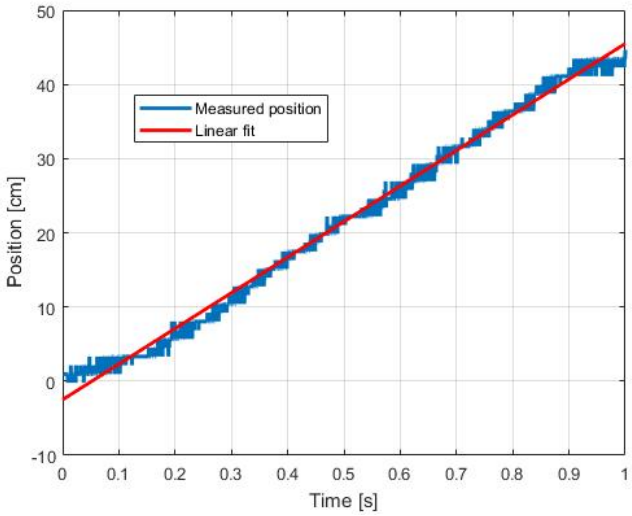

Figure 19: Position obtained from the draw-wire sensor (blue) and a linear fit (red). The slope obtained from the linear fit is used in the COMSOL model.

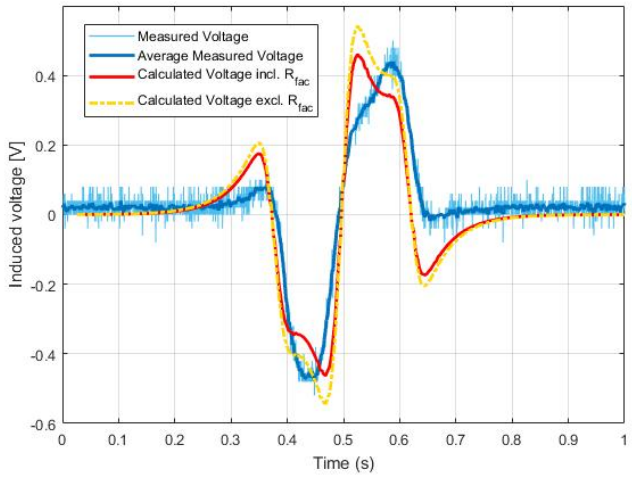

Figure 20: Induced voltage obtained from measurement (blue) and from the numerical model (red). Dashed yellow line shows the calculated voltage without the factor adjusting the magnets' remanent flux density.

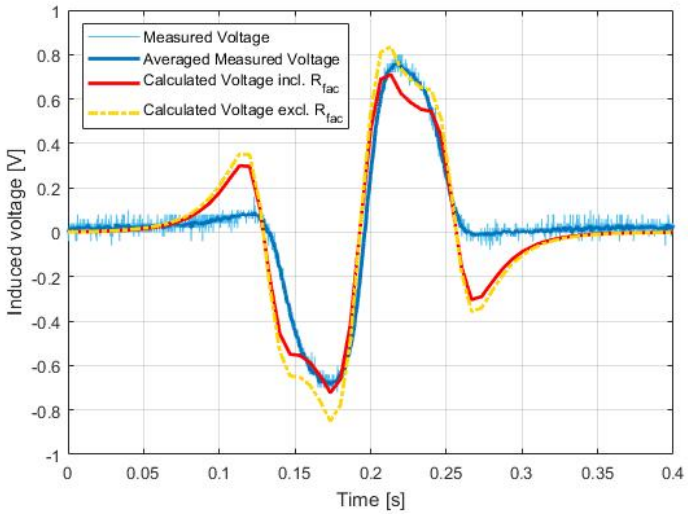

Figure 21: Induced voltage for the test case with speed 0.89 m/s. Blue lines obtained from measurement and the red line is the numerically calculated voltage.

4.4 Stator iron

To make the prototype testing a little more interesting, a small piece of soft iron was put outside of the coil. The piece was 1mm thick and 35mm high, covering just over half of the height of the coil and fitting closely on the outside of the coil. There was a noticeable difference in the way the translator moved in this case, we noticed large attractive forces due to this relatively small piece of soft iron, making the translator stick in the middle of the coil. Figure 22 show the measured position with both a linear fit and a piecewise linear fit. This also revealed how sensitive the induced voltage is to velocity, a small deviation from smooth linear motion gives a noticeable difference in the peak voltage, see Figure 23. The numerical model does capture the qualitative behaviour when using the piecewise linear motion.

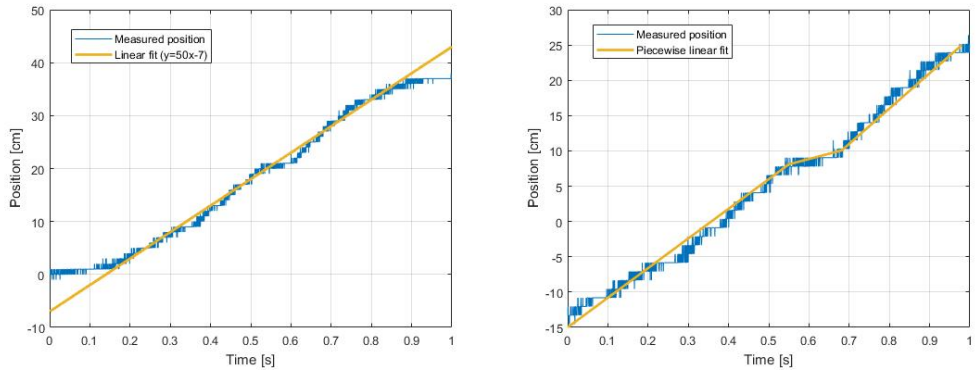

Figure 22: Measured position for a test case when the translator stuck. Simple linear fit to the left and piecewise linear fit to the right.

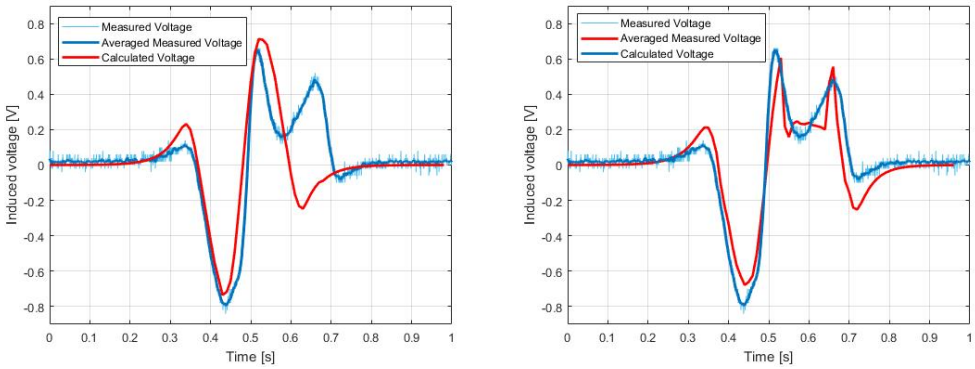

Figure 23: Measured and calculated induced voltage for the simple linear fit on the left and piecewise linear fit on the right.

5 Full size generator model

This section describes the numerical model of the suggested design for the full scale generator and the resulting magnetic fields, power output and efficiency. The model is essentially the same as the one used for the experimental verification, it is 2D axisymmetric with solid magnets when in reality it has many smaller individual magnets in each row. The magnets are larger compared to the ones used in the experimental set up and the translator has 24 magnets in four rows. The parameters used can be found in Table 2 and in Figure 24.

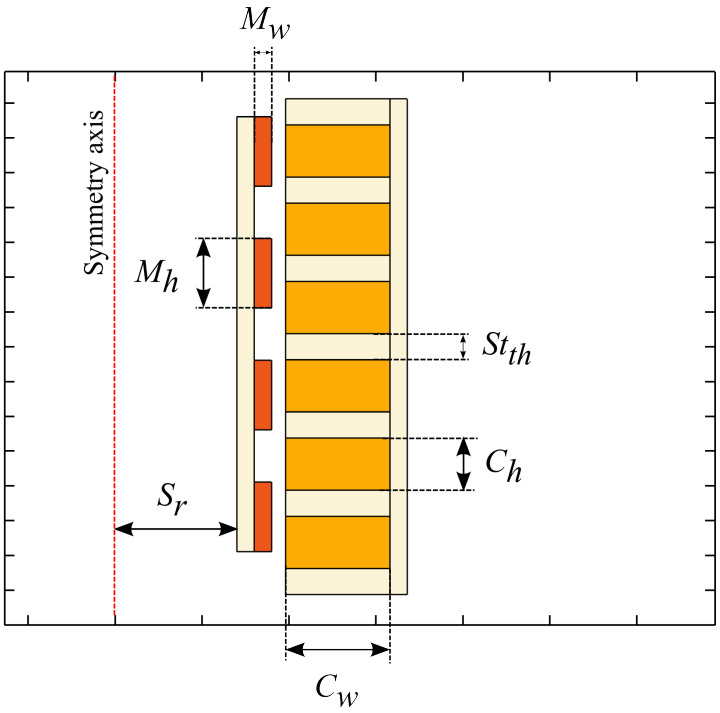

Figure 24: Definition of the different model parameters.

5.1 Magnetic fields and induced voltage

It is the changing magnetic field that induces a voltage in the coils so it is essential that we know how the magnetic flux density behaves. The norm of the magnetic flux field is shown in 2D in Figure 25 and snapshots of three different instances in time in 3D is shown in Figure 26. The air gap magnetic flux

density can be estimated using Eq.(20). The flux density (rz-plane) in the air gap between an aligned magnet and stator tooth, assuming $\mu_{fe} = 1000$, is found to be $B_a = 0.76$ T. The numerical simulation gives the maximum value of B_a as around 0.8 T. This occurs when the magnets and stator teeth are aligned.

The current densities in the generator coils are shown in Figure 27. At this instance in time the translator is moving downwards so that the top and bottom coils have a negative direction for the current and the middle coil positive. Considering the position of the magnets we can see that this is the direction which induces a magnetic field opposing the motion according to Lenz law.

Figure 28 shows the induced voltage in the two middle coils over a 5 second interval. These can be seen to be phase shifted and the highest voltages induced for the highest velocity, c.f. Figure 11. A 60 second plot of the induced voltage in one coil is shown in Figure 29, where the irregular, sharp spikes of the coil voltage on the longer time scale are clearly displayed.

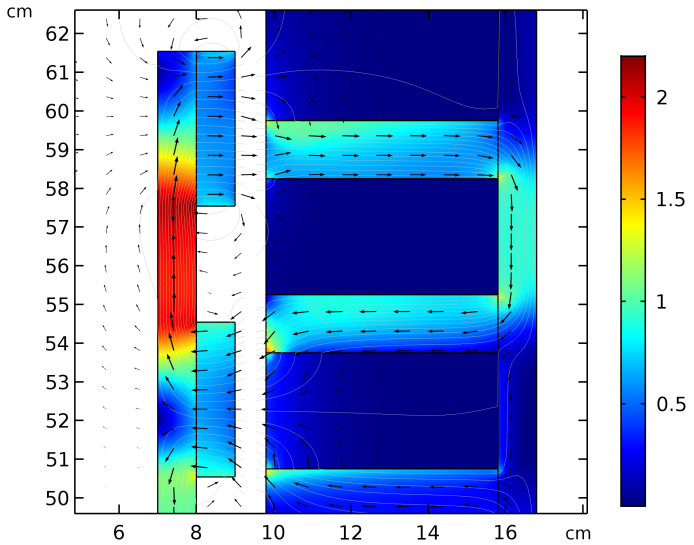

Figure 25: Magnetic flux density norm (T).

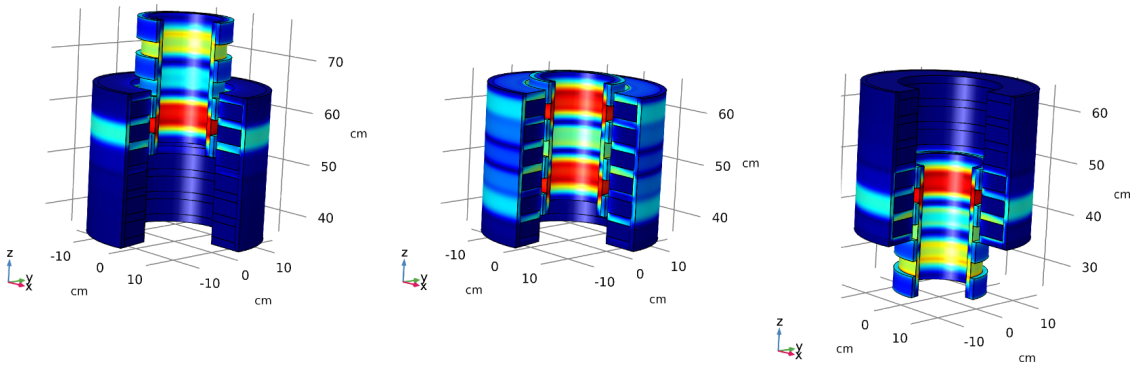

Figure 26: Magnetic flux density norm at half a second intervals (T).

Table 2: Model parameters. Parameter definitions in Figure 24.

Symbol	Value	Description
M_h	40 mm	Magnet height
M_w	10 mm	Magnet width
C_h	30 mm	Coil height (cross section)
C_w	30 mm	Coil width (cross section)
S_r	80 mm	Inner shaft radius
St_{th}	15 mm	Stator tooth height
R_g	0.86 Ω	Coil resistance for each phase
L_g	17.5 mH	Coil inductance
V_{rms}	6.23 V	RMS voltage in coil 1 over the 5 s interval
R_{fac}	0.9	Factor adjusting for individual rather than solid magnets
m_t	17.6 kg	Mass of the translator
γ	500 Ns/m	Assumed damping coefficient

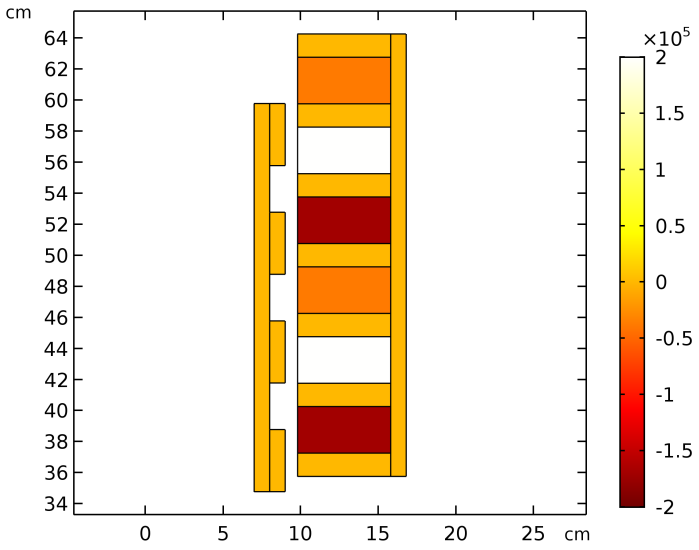

Figure 27: ϕ-component of the current density ($\mathrm{A/m^2}$). Positive ϕ-direction going into the page. Arbitrary scale for current density, only to show the direction of the induced current.

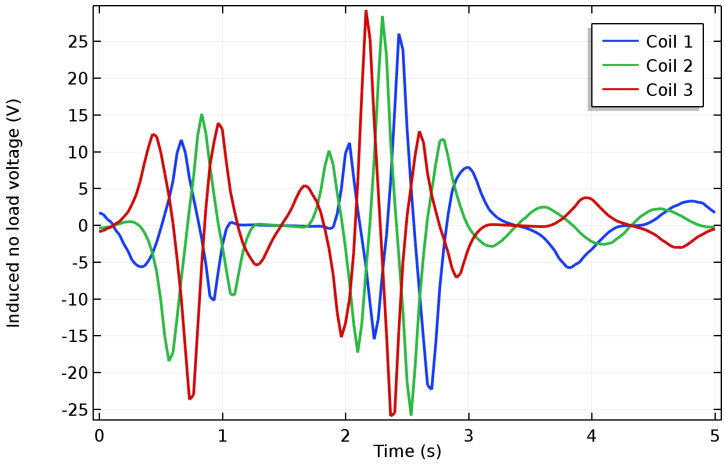

Figure 28: Induced voltage in the three coils.

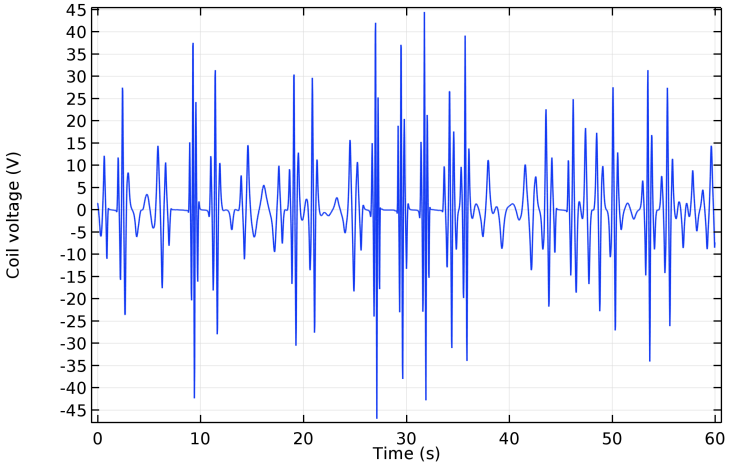

Figure 29: Induced voltage over a 60 second interval.

5.2 Power, damping and efficiency

The power output from the generator is the power consumed in an external load, in this case a single resistive load, see Figure 7, that represents charging of batteries. The efficiency η is defined as the ratio of the power consumed in the load and the power input from the buoy given a specific damping coefficient:

$$\eta = \frac{P_{load}}{P_{in}}. \tag{27}$$

In the way this model is made, the external loading must be balanced so that the damping coefficient corresponds to the one used for the input position of the buoy, here 500 Ns/m. This is done by matching the sum of the average power in the coils and in the load, with the power input given by the assumed damping coefficient. The power losses in the coils are fixed, while the power in the load is determined by the load resistance.

The power output is displayed in Figure 30 for a load resistance of 11 Ω. The average power in the load over the 5 second interval is 14.1 W, additionally 2.1 W is lost in the coils (coil resistance 0.86 Ω per phase). The power absorbed by the bouy is 16.4 W, giving an overall efficiency of 86%. However, this efficiency only accounts for the power loss in the coils and in addition there is a large uncertainty in the inductance of the coils. The value for the inductance is calculated using Eq.(25), assuming a simple air-cored coil. It has also been calculated a few different ways [30, 31], with varying results but still giving the order of magnitude as tens of mH.

The calculated damping force is shown in Figure 31. The blue line shows the force obtained using the power calculated in COMSOL (Eq.(23)) and the green line is the force calculated from the input velocity and damping coefficient of 500 Ns/m (Eq.(6)). The average power over the time interval is the same for the two, but it's clearly seen that the force calculated from the power has higher but more narrow peaks. It is expected that the actual damping will be greater than this due to friction and loss processes such as eddy currents induced in the stator iron.

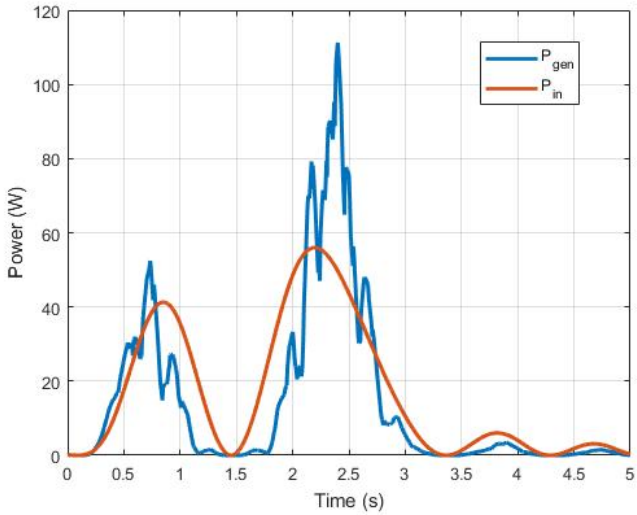

Figure 30: Total power from the six coils (blue) and the power assuming $\gamma = 500$ Ns/m.

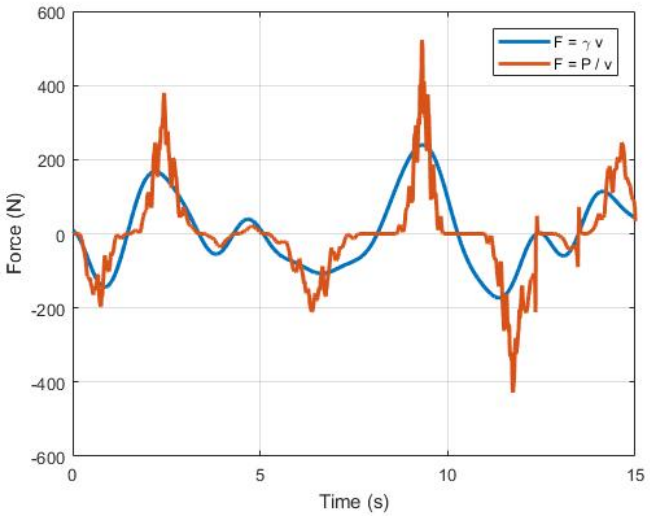

Figure 31: Damping force calculated from the power obtained from the power (red) and from the input velocity assuming $\gamma = 500$ Ns/m (blue).

5.3 Parameter dependence

Parametric analyses on a tubular linear generator was performed in Ref.[37]. It found that pole pitch (distance between magnets), height of the stator, coil thickness and magnet thickness have the largest influence on the magnitude of the flux through the stator iron. To find out how different parameters influence the average power obtained for this generator model, a number of parametric sweeps were performed. The only design constraints are a maximum diameter of 35 cm and that the weight of the translator should be 20 kg. The different magnet sizes considered were ones readily available from the supplier. When actually constructing the generator, a number of additional criteria might need to be satisfied. The geometry, materials or design will likely be changed in order to accommodate for example economical or practical aspects. For this reason, it is desirable to study the effects of different parameters and if possible identify key parameters/indicators for high efficiency to speed up the design process. The following sections describe the different parameters that have been studied.

5.3.1 Coil geometry

The coil area and the height of the space between the magnets have been varied by performing a large parameter sweep in COMSOL. 18 different cases were then run through Simulink to find the efficiency. From this a number of parameters were Figure 32 shows that the efficiency is very well accounted for by using the RMS voltage from one coil divided by the coil resistance. To get a quick estimate of the performance of the generator it is therefore sufficient to find and compare the RMS voltage and coil resistance only, without having to run the Simulink simulation.

In the model, the available coil area determines the number of coil winding turns given a specific cable size. That is, as many coil turns as possible is fitted in the available area. Increasing the number of coil windings increases the induced voltage linearly but the coil resistance and inductance also increases. To achieve a high efficiency, a balance between the two should be found. The parameter sweep showed a large variation in efficiency, the lowest efficiency being 10% while the highest was 86%. Figure 33 shows that the RMS value of the induced voltage (in one coil) and the coil resistance has a seemingly linear dependence on the coil width. It is on the other hand

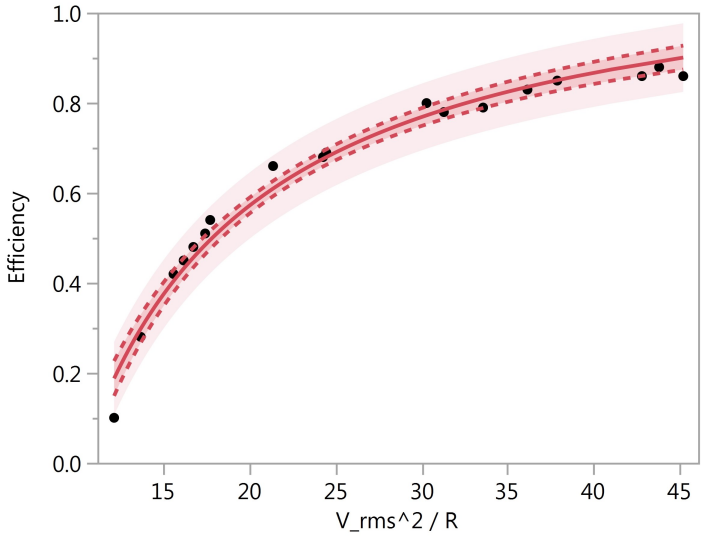

Figure 32: Efficiency as a function of the RMS voltage squared divided by coil resistance.

largely uninfluenced by the coil height and the height of the space between the magnets.

5.3.2 Magnet geometry

A few different magnet sizes have been tested and the RMS voltage is shown in Figure 34. It is clear that a larger magnet cross sectional area induces a higher voltage, however larger magnets also increases the translator mass, which is restricted to 20 kg.

5.3.3 Stator iron thickness

The back iron thickness and the height of the stator teeth has been varied and the RMS voltage from one coil evaluated for the different cases. The coil resistance is constant so it is sufficient to consider only the RMS voltage. The result is shown in Figure 35, the stator tooth height has a clear maximum for 17.5 mm while the stator back iron thickness in this range barely influences the induced voltage.

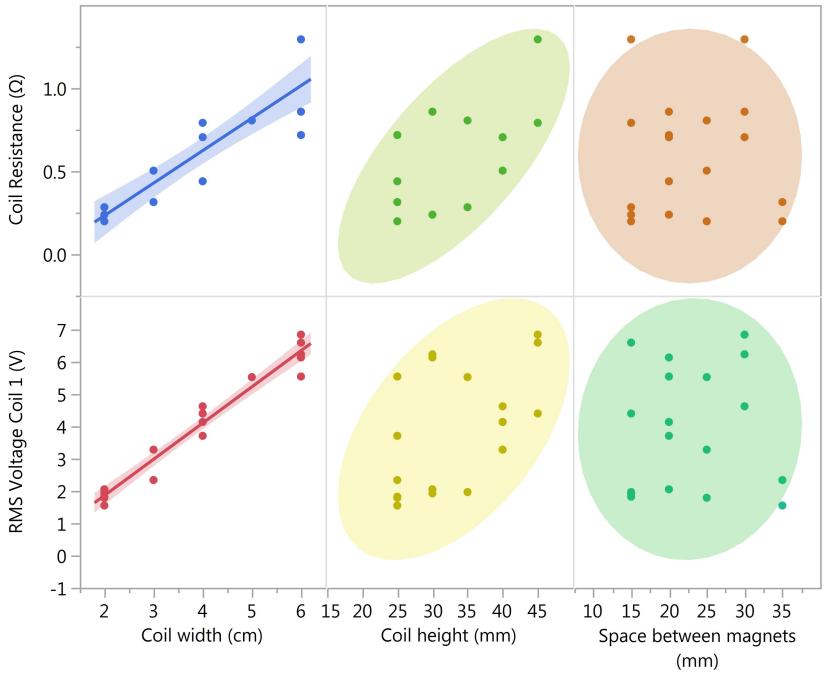

Figure 33: The coil width (far left) has a linear correlation with the RMS voltage and coil resistance while the coil height and space between magnets are largely uncorrelated.

5.3.4 Cable size

Having more coil turns increases the voltage linearly, however the coil resistance increases both with decreasing cable cross section area and the length of the coil. The inductance will also be affected. Using the estimate in Eq.(25), the inductance increases quadratically with the number of coil turns.

Three different cable cross sections were tested and showed that a balance between number of turns and coil resistance achieved the highest efficiency, see Table 3. Cost and availability will also be a factor in choosing the cables.

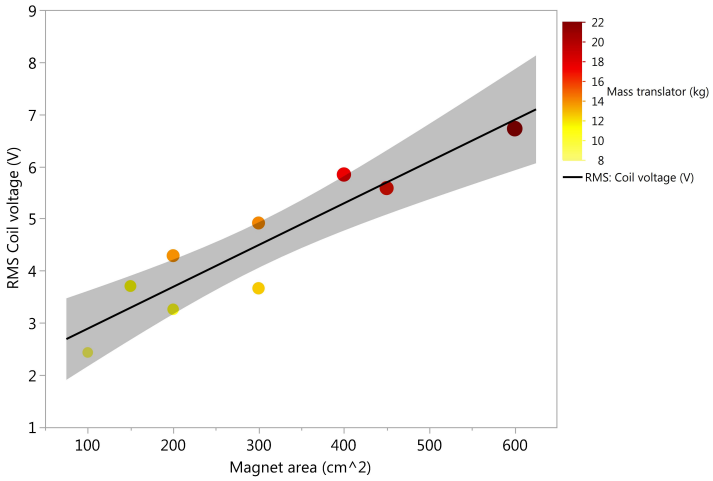

Figure 34: RMS value of the no load voltage in coil 1 for the different magnet sizes with a fitted linear function. The mass of the translator is indicated by the colour of the dots.

Table 3: Three different sized cables used in the coils. The efficiency here is defined as the ratio of power in the load and the power loss in the coil windings: $P_{load}/(P_{load} + P_{loss})$.

Cable diameter (mm^2)	Number of turns	Coil resistance (Ω)	Efficiency
2.5	159	1.7	0.84
4	128	0.86	0.87
10	44	0.18	0.79

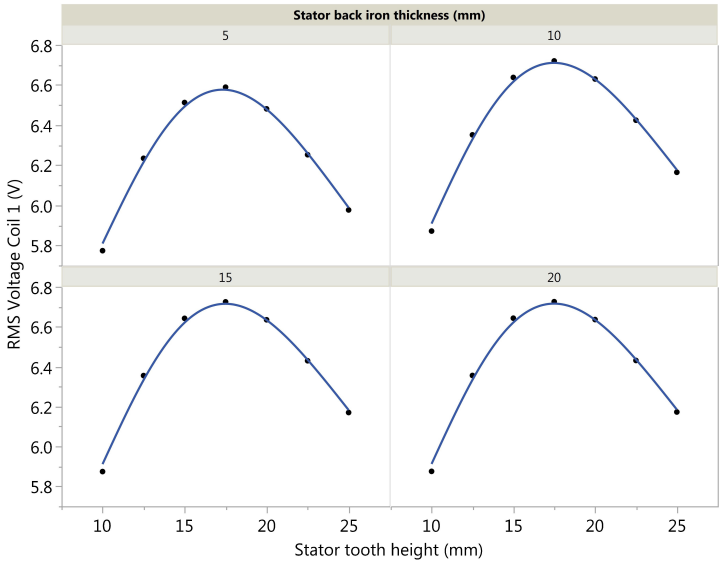

Figure 35: RMS voltage for different stator tooth height and stator back iron thicknesses.

5.3.5 Current in stator and core iron

The model has also been run with non-ideal soft iron, where the electrical conductivity $\sigma = 1.12 \times 10^7$ S/m. This means that currents are induced in the stator iron, see Figure 36. The effect is a slightly lower efficiency, one percentage point, compared to the ideal material. However, the efficiency is in reality lower since the extra power loss and subsequent extra damping is not included. Thus we cannot match the damping, rendering the simulation results invalid. It is difficult to calculate the effect of the eddy currents, however, the stator iron for generators in general is commonly laminated and the power loss using laminated sheets can be estimated according to Eq.(22). We assume a constant frequency of 1.5 Hz for the wave motion and 1 mm thick laminates. A maximum magnetic flux density of 2.4 T was obtained from the model and we then get

$$P_{loss}^{eddy} = 1.12 \times 10^7 \text{ S/m} \left[(\pi 1.5\text{Hz}) \times 1\text{mm} \times 2.4\text{T}\right]^2 /6 = 239\text{W/m}^3. \quad (28)$$

This gives a total of 2.1 W over the volume of the iron in the stator. Considering that this is the same magnitude as the resistive losses, it is not insignificant and warrants further study.

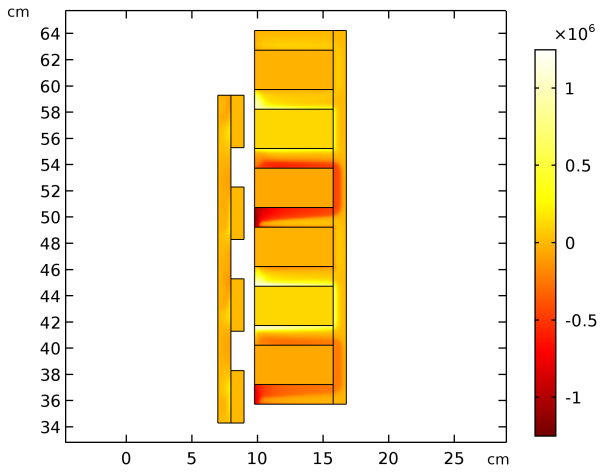

Figure 36: Current density when including electrical conductivity of the stator iron.

6 Discussion and conclusions

The experimental tests show close correspondence between the numerical model and the measured values. The factor used to compensate for the missing magnet volume in the real set up compared to the model seems to be able to account for the, albeit small, difference. However, most of the interesting behaviour when including stator iron, several coils and the electrical circuit has not been evaluated and the accuracy of the full model cannot be fully inferred from these experimental tests.

In the full model and electrical circuit, the power output is matched with that expected from the assumed damping coefficient by varying the load resistance. The matching is done using the average value over the time interval. The simulated damping is found to be more narrowly peaked than the corresponding assumed damping while having the same average power. This is at least in part due to the short stator length, since the translator moves completely outside of the stator for part of the stroke. This does not have a significant effect on the average power obtained since the translator moves much slower at the ends of the strokes, i.e. providing less power.

However, in the experimental test there was a noticeable difference in the force required to pull the translator past the coil with only a small piece of stator iron wrapped around the coil. Solid support structures will be required to keep the translator aligned, but the end effects might still be so significant that it warrants a longer stator. Adding more coils and making the stator longer would not adversely affect the power output, so it could be tested and evaluated while the translator is being built. Another option is to include end stops or springs limiting the length of the stroke and thus reducing these nonlinear end effects while keeping a short stator. In this project the translator weight was limited to 20 kg. It is however not strict, the hydrodynamic modelling can simply be redone if required.

Parametric sweeps found that coil width and magnet area were most decisive for the induced voltage and generator efficiency. The efficiency can be well predicted with the RMS value of the induced voltage and the coil resistance. Thus it is possible to use this value calculated directly in COMSOL for optimisation purposes, rather than having to run the Simulink model each time as well. The power output is found to be very sensitive to design param-

eters, the efficiency was seen to vary between 10% and 86%. The size of the cables in the coils also influences the efficiency but can easily be optimised within the model. For a given magnet size an optimal stator tooth height was found, while the stator back iron thickness was largely unimportant for the efficiency.

In addition to the influence of design parameters, there are several sources of uncertainty. Notably the inductance used in the circuit simulations and the effect of eddy currents in the stator iron. For the former, several different estimates give the inductance within the same order of magnitude; tens of mH. Variations in the inductance of this magnitude was found to change the efficiency by a few percentage points.

The currents induced in the stator iron when assuming a solid piece of iron can be simulated using the model. However, this is not useful since the extra damping is not included and the resulting motion of the translator (and thus power output) cannot be determined. Instead, an estimate of the power loss when using laminated sheets showed that it is of similar magnitude to the resistive power loss in the coils and will if so be a significant source of power loss. Hysterisis losses can be calculated when choosing the exact materials.

In conclusion, there are too many unknowns and assumptions to say if this design will provide the required output based on this model alone. The model could however be used concurrently while building the generator to check for example the qualitative behaviour of changing some dimensions or materials. In general this type of model is more useful to be able to identify important parameters of the construction, rather than providing a final design.

6.1 Future research

For the next stage of the construction, the support structure, ends stops and integration with the main buoy needs to be designed. In addition there are many unexplored parts of the generator that are still to be investigated, for example the exact geometries and materials used, as well as cost. Once the generator is constructed wave tests in the tank can be performed.

It is also possible to investigate and compare alternative PTO systems. It could for example be possible to utilise the tilting motion of the main buoy, inertial mass movement, this has the advantage of being completely enclosed inside the main buoy [38] . It is uncertain whether this would provide enough power and data of main buoy movement required to evaluate this. One could also consider and test a linear-to-rotary conversion system attached to a conventional rotary generator, for example one of the systems in Ref.[7].

Acknowledgements

First and foremost I would like to thank Rafael Waters, Mohd Nasir Ayob and the Department of Electricity for the opportunity to perform this thesis project. I would also like to specifically thank my supervisor Mohd Nasir Ayob for all his help and positive attitude during the project. Thanks also to Valeria Castellucci for your input and the magnets.

I would like to express my gratitude to my family for all the support and encouragement, both during this project and during the past years of studying leading up to this thesis. I am especially thankful for the support from my parents, I dedicate this thesis to you.

References

[1] Valeria Castellucci. "Sea Level Compensation System for Wave Energy Converters". PhD thesis. Uppsala University, 2016.

[2] Rafael Waters. "Energy from Ocean Waves: Full Scale Experimental Verification of a Wave Energy Converter". PhD thesis. Uppsala University, 2008.

[3] Iraide López et al. "Review of wave energy technologies and the necessary power-equipment". In: *Renewable and Sustainable Energy Reviews* 27 (2013), pp. 413–434.

[4] Aamir Hussain Memon, Taib bin Ibrahim, and Perumal Nallagowden. "Design Optimization of Linear Permanent Magnet Generator for Wave Energy Conversion". In: 2015 IEEE Conference on Energy Conversion (CENCON). 2015. DOI: 10.1109/CENCON.2015.7409561.

[5] Emre Ozkop and Ismail H. Altas. "Control, power and electrical components in wave energy conversion systems: A review of the technologies". In: *Renewable and Sustainable Energy Reviews* 67 (2017), pp. 106–115. DOI: http://doi.org/10.1016/j.rser.2016.09.012.

[6] Rickard Ekström, Boel Ekergård, and Mats Leijon. "Electrical damping of linear generators for wave energy converters—A review". In: *Renewable and Sustainable Energy Reviews* 42 (2015), pp. 116–128.

[7] K. Rhinefrank et al. "Comparison of Direct-Drive Power Takeoff Systems for Ocean Wave Energy Applications". In: *IEEE Journal of Oceanic Engineering* 37.1 (2012), pp. 35–44.

[8] S. Chiba et al. "Consistent ocean wave energy harvesting using electroactive polymer (dielectric elastomer) artificial muscle generators". In: *Applied Energy* 104 (2013), pp. 497–502.

[9] Bret Bosma et al. "Wave Tank Testing and Model Validation of an Autonomous Wave Energy Converter". In: *Energies* 8 (2015), pp. 8857–8872. DOI: http://doi:10.3390/en8088857.

[10] J.C.C. Henriques et al. "Design of oscillating-water-column wave energy converters with an application to self-powered sensor buoys". In: *Energy* 112 (2016), pp. 852–867.

[11] Deanelle Symonds, Edward Davis, and R. Cengiz Ertekin. "Low-Power Autonomous Wave Energy Capture Device for Remote Sensing and Communications Applications". In: 2010 IEEE Energy Conversion Congress and Exposition. 2010, pp. 2392–2396. DOI: 10.1109/ECCE.2010.5617902.

[12] Inc. Ocean Power Technologies. *PowerBuoy Technology - Ocean Power Technologies*. URL: http://www.oceanpowertechnologies.com/powerbuoy-technology/ (visited on Apr. 27, 2017).

[13] MBARI Monterey Bay Aquarium Research Institute. *Wave-Power Powerbuoy*. URL: http://www.mbari.org/technology/emerging-current-tools/power/wave-power-buoy/ (visited on Apr. 27, 2017).

[14] Cecilia Boström. "Electrical Systems for Wave Energy Conversion". PhD thesis. Uppsala University, 2011.

[15] Avdelningen för elektricitetslära. *Vågkraft - Institutionen för teknikvetenskaper - Uppsala Universitet*. URL: http://www.teknik.uu.se/elektricitetslara/forskningsomraden/vagkraft/ (visited on Aug. 9, 2017).

[16] V. Castellucci et al. "Influence of Sea State and Tidal Height on Wave Power Absorption". In: *IEEE Journal of Oceanic Engineering* 99 (2016), pp. 1–8. DOI: 10.1109/JOE.2016.2598480.

[17] Mohd Nasir Ayob, Valeria Castellucci, and Rafael Waters. "Tidal Effect Compensation System Design for High Range Sea Level Variations". In: Proceedings of the 11th European Wave and Tidal Energy Conference 6-11th Sept 2015, Nantes, France. 2015.

[18] Tsutomu Kambe. *Elementary fluid mechanics*. London;Hackensack, N.J; World Scientific, 2007.

[19] M. Eriksson, J. Isberg, and M. Leijon. "Hydrodynamic modelling of a direct drive wave energy converter". In: *International Journal of Engineering Science* 43 (2005), pp. 1377–1387.

[20] Liselotte Ulvgård et al. "Line Force and Damping at Full and Partial Stator Overlap in a Linear Generator for Wave Power". In: *Journal of Marine Science and Engineering* 4 (81 2016). DOI: doi:10.3390/jmse4040081.

[21] David J. Griffiths. *Introduction to Electrodynamics*. Pearson Education Inc., 2008.

[22] Göran Jönsson. *Tillämpad ellära*. Första upplagan. Lund: Teach Support, 2015.

[23] Thomas S. Parel et al. "Optimisation of a tubular linear machine with permanent magnets for wave energy extraction". In: *COMPEL: The International Journal for Computation and Mathematics in Electrical and Electronic Engineering* 30.3 (2011), pp. 1056–1068. DOI: 10.1108/03321641111110997.

[24] K. Nilsson, O Danielsson, and M. Leijon. "Electromagnetic forces in the air gap of a permanent magnet linear generator at no load". In: *Journal of Applied Physics* 99 (034505 2006). DOI: 10.1063/1.2168235.

[25] Nathan Michael Tom. "Design and Control of a Floating Wave-Energy Converter Utilizing a Permanent Magnet Linear Generator". PhD thesis. University of California, Berkeley, 2013.

[26] R. Vermaak and M. J. Kamper. "Design Aspects of a Novel Topology Air-Cored Permanent Magnet Linear Generator for Direct Drive Wave Energy Converters". In: *IEEE Transactions on Industrial Electronics* 59.5 (2012), pp. 2104–2115. DOI: 10.1109/TIE.2011.2162215.

[27] Boel Ekergård et al. "Experimental results from a linear wave power generator connected to a resonance circuit". In: *WIREs Energy Environ* 2 (2013), pp. 456–464. DOI: 10.1002/wene.19.

[28] J.K.H. Shek et al. "Reaction force control of a linear electrical generator for direct drive wave energy conversion". In: *IET Renewable Power Generation* 1 (1 2007).

[29] M. Eriksson et al. "Wave power absorption: Experiments in open sea and simulation". In: *Journal of Applied Physics* 102 (084910 2007). DOI: http://dx.doi.org/10.1063/1.2801002.

[30] Boel Ekergård, Rafael Waters, and Mats Leijon. "Prediction of the Inductance in a Synchronous Linear Permanent Magnet Generator". In: *Journal of Electromagnetic Analysis and Applications* 3 (2011), pp. 155–159. DOI: 10.4236/jemaa.2011.35025.

[31] John E. Lane et al. *Magnetic Field, Force, and Inductance Computations for an Axially Symmetric Solenoid Magnetic Field, Force, and Inductance Computations for an Axially Symmetric Solenoid*. NASA/TM-2013-217918. 2001.

[32] J. N. Reddy. *An introduction to the finite element method*. 3rd ed. Boston: McGraw-Hill, 2006.

[33] Jeong-Man Kim et al. "Design and analysis of tubular permanent magnet linear generator for small-scale wave energy converter". In: *AIP Advances* 7.5 (2017), p. 056630. DOI: 10.1063/1.4974496.

[34] Joseph Prudell et al. "A Permanent-Magnet Tubular Linear Generator for Ocean Wave Energy Conversion". In: *IEEE TRANSACTIONS ON INDUSTRY APPLICATIONS* 46.6 (2010).

[35] M. G. Park et al. "Electromagnetic Analysis and Experimental Testing of a Tubular Linear Synchronous Machine With a Double-Sided Axially Magnetized Permanent Magnet Mover and Coreless Stator Windings by Using Semianalytical Techniques". In: *IEEE Transactions on Magnetics* 50.11 (2014), pp. 1–4. DOI: 10.1109/TMAG.2014.2323957.

[36] V. DelliColli et al. "A Tubular-Generator Drive For Wave Energy Conversion". In: *IEEE Transactions on Industrial Electronics* 53.4 (2006), pp. 1152–1159.

[37] A. Pirisi, G. Gruosso, and R. E. Zich. "Novel modeling design of three phase tubular permanent magnet linear generator for marine applications". In: *2009 International Conference on Power Engineering, Energy and Electrical Drives*. 2009, pp. 78–83. DOI: 10.1109/POWERENG.2009.4915209.

[38] Jeffrey T. Cheung. *Frictionless Linear Electrical Generator for Harvesting Motion Energy*. 2004.